# Journal of Materials Chemistry C

Accepted Manuscript


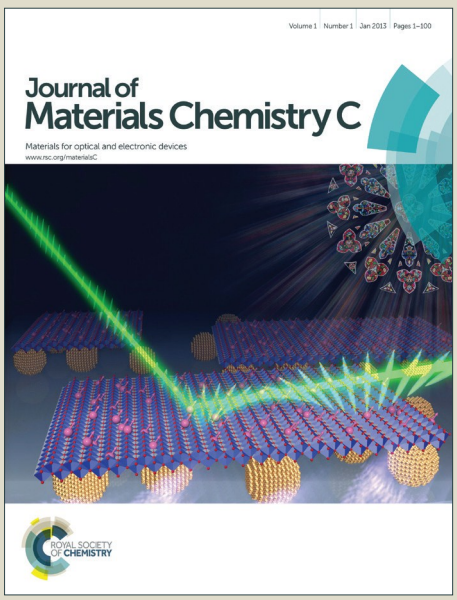





ROYAL SOCIETY OF CHEMISTRY

www.rsc.org/materialsC

Journal of Materials Chemistry C

COMMUNICATION

# Synthesis, Properties, and OLED Characteristics of 2,2′-Bipyridine-Based Electron-Transport Materials: Synergistic Effect of Molecular Shape Anisotropy and a Weak Hydrogen-Bonding Network on Molecular Orientation†

Received 00th January 20xx,
Accepted 00th January 20xx

DOI: 10.1039/x0xx00000x

www.rsc.org/

Yuichiro Watanabe,[a] Hisahiro Sasabe,*[a,b] Daisuke Yokoyama,[a,b] Teruo Beppu,[a] Hiroshi Katagiri,[a,b] and Junji Kido*[a,b]

**To boost the performances of OLEDs, one of the most promising approaches from a materials chemistry viewpoint is the use of thin solid films with horizontal molecular orientations. In this work, we developed 2,2′-bipyridine-skeleton-based electron-transport materials (ETMs) end-capped with 3,5-dipyridylphenyl groups with the objective of preparing films with horizontal molecular orientations for use in high-performance organic light-emitting devices (OLEDs). These compounds afforded highly oriented films and were used in *fac*-tris(2-phenylpyridine)iridium(III)-based OLEDs as an ETL. The optimized device exhibited low operating voltages of 2.8 and 3.2 V at luminances of 100 and 1000 cd $m^{-2}$, respectively. At 1000 cd $m^{-2}$, this device exhibited a power efficiency of 74 lm $W^{-1}$ and an external quantum efficiency of 21%.**

Organic light-emitting devices (OLEDs) have been widely used in flat-panel displays in smart phones, smart watches, and large-screen televisions and are expected to become the next eco-friendly solid-state lighting technology.[1] From a materials chemistry perspective, one approach to boost the performance of OLEDs, where one should use not a crystalline film but an amorphous thin solid film, is the use of horizontal molecular orientations.[2] However, controlling the molecular orientation in an amorphous thin film has been an underexplored topic throughout the past decade, even though researchers have intensively investigated the electronic and optical properties of single molecules. Recently, the molecular orientations of hole-transport materials (HTMs) and emissive materials based on carbazole and triphenylamine derivatives have been systematically investigated.[3] For example, Yokoyama and co-workers investigated the molecular orientations of a series of carbazole derivatives using variable-angle spectroscopic ellipsometry (VASE) analysis.[3a] Consequently, they found that molecular shape anisotropy is important for horizontal orientation and that linear and long-shaped molecules tend to be more horizontally oriented than nonlinear and short-shaped molecules. In addition, Wakamiya and co-workers reported that quasiplanar, partially oxygen-bridged triarylamines with linear and long molecular shapes exhibit a horizontal orientation.[3b]

By contrast, our group focused on the active control of the molecular orientation through CH···N weak hydrogen bonding (H-bonding) of peripheral pyridine rings in addition to π–π stacking.[4] For example, we recently developed a 1,3,5-triphenyltriazine derivative called BPyPTZ, which exhibits both intramolecular and intermolecular H-bonding abilities, to attain the highest order of horizontal molecular orientation in electron-transport materials (ETMs).[5] In this regard, the combination of molecular shape anisotropy and H-bonding ability represents a promising approach to horizontally orient a molecule in an amorphous film. We introduced a 2,2′-bipyridine (BPy) skeleton, which induces effective stacking by steric repulsion of hydrogen atoms and electron repulsion of lone pairs,[6] into the molecule to make the molecular shape linear.[7] With respect to the intermolecular H-bonding networks, we introduced two bipyridylphenyl moieties onto the end of the molecule. We named these novel series of ETMs as BPy derivatives (4,4′-BPy3 and 6,6′-

[a] *Department of Organic Device Engineering, Graduate School of Science and Engineering, Yamagata University, Yonezawa, Yamagata, 992-8510 Japan.*
[b] *Research Center for Organic Electronics (ROEL), Yamagata University, Yonezawa, Yamagata, 992-8510 Japan.*
†We thank Dr. T. Chiba, Mr. T. Ide, Mr. S. Kagami and Ms. C. Katagiri (Yamagata University) for technical support in time of flight measurements and electron only device measurements.
This study was partially supported by the Center of Innovation Program from Japan Science and Technology Agency, JST and by Japan Society for the Promotion of Science, JSPS KAKENHI Grant Numbers 26620202, 15J08167.
Electronic Supplementary Information (ESI) available: [details of any supplementary information available should be included here]. See DOI: 10.1039/x0xx00000x.

BPy3). The BPy skeleton was installed to form intramolecular H-bonding, which enables molecular shape anisotropy (**Figure 1**). The peripheral pyridine rings provide weak intermolecular H-bonding ability to complementally support a π–π stacking. We expect a synergistic effect between shape anisotropy and weak intermolecular interaction to afford substantial horizontal molecular orientation, thereby realizing high electron mobility and leading to OLEDs with a low operating voltage and high power efficiency.

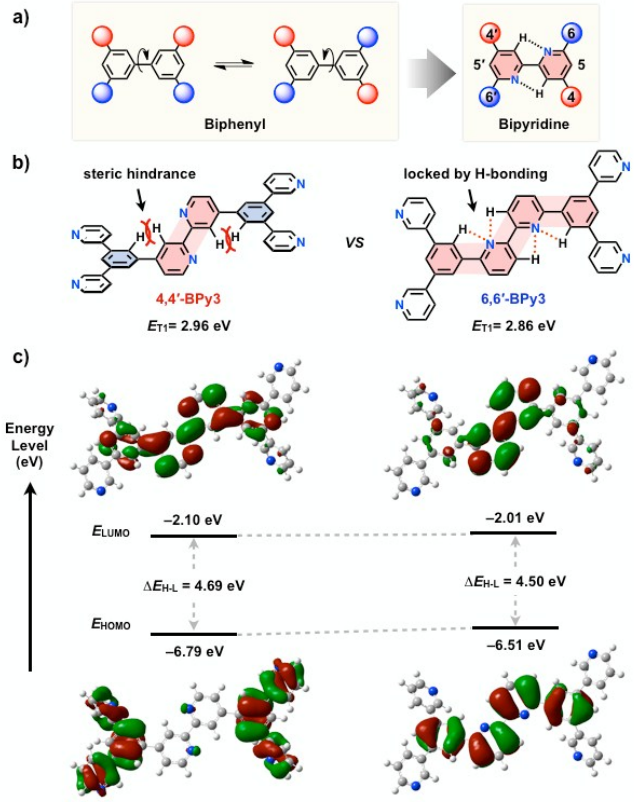


**Figure 1**. a) Concept of the 2,2′-bipyridine-skeleton-based electron-transport materials and b) chemical structures of 4,4′-BPy3 and 6,6′-BPy3. c) The calculated spatial distributions of the HOMOs and LUMOs for the BPy derivatives at the RB3LYP 6-311+G(d,p)//RB3LYP 6-31G(d,p) level.

Prior to preparing 4,4′-BPy3 and 6,6′-BPy3, we conducted density functional theory (DFT) calculations to estimate the effect of substitutions of the BPy molecular framework. An optimized structure was calculated at the RB3LYP 6-31G(d,p) level for the ground state. The single-point energies were calculated at the corresponding RB3LYP 6-311+G (d,p) levels. The optimized molecular structure of 4,4′-BPy3 exhibited contortion around the phenyl group attached to the BPy moiety. Because of this twisted structure, the calculated highest occupied molecular orbital (HOMO) localized peripheral 3,5-dipyridylphenyl moieties. By contrast, 6,6′-BPy3 exhibited a more planar molecular framework that led to spreading of the HOMO around the molecular framework (**Figure 1c**). The HOMO energy of the BPy derivatives were estimated to be −6.79 eV for 4,4′-BPy3 and −6.51 eV for 6,6′-BPy3, which are deeper than the HOMO of conventional ETMs. The corresponding lowest unoccupied molecular orbitals (LUMOs) were mainly distributed on the BPy moiety; these energies were evaluated to be −2.10 eV for 4,4′-BPy3 and −2.01 eV for 6,6′-BPy3, which are also much deeper than those of conventional ETMs, suggesting a better electron-injection property.[8] We also calculated the triplet energy ($E_T$) from Time-dependent DFT calculations at the RB3LYP 6-31G(d,p) level using the aforementioned optimized structure. The $E_T$ levels were evaluated to be as high as approximately 2.90 eV, which is applicable for blue and green phosphorescent and thermally activated delayed-fluorescence-type OLEDs. All of the calculated data are summarized in **Table S1**.

The synthetic route to the BPy derivatives is shown in **Scheme S1** in the supporting information (**SI**). All the BPy derivatives were easily prepared on a multigram scale in two steps from dibromo-2,2′-bipyridine. The precursor tetrachloride was prepared in almost 50% yield via the Suzuki–Miyaura cross-coupling reaction of 4,4′-dibromo-2,2′-bipyridine or 6,6′-dibromo-2,2′-bipyridine with 3,5-dichlorophenyl boronic acids. The resulting tetrachloride precursors were coupled with an excess of 3-pyridine boronate ester in the presence of tris(dibenzylideneacetone)-dipalladium(0) [$Pd_2(dba)_3$] and 2-dicyclohexylphosphino-2′,6′-dimethoxybiphenyl (S-Phos) to give 4,4′-BPy3 in 81% yield and 6,6′-BPy3 in 92% yield, respectively. All compounds were characterized by Thin-layer chromatography (TLC) analysis on silica gel, $^1$H NMR spectroscopy, mass spectrometry, and elemental analysis (see **SI**). Moreover, single-crystal X-ray structure determinations were performed for 4,4′-BPy3 and 6,6′-BPy3. These compounds exhibit high thermal stabilities. The thermal properties of the BPy derivatives were estimated by differential scanning calorimetry (DSC) and thermogravimetric analysis (TGA). 4,4′-BPy3 and 6,6′-BPy3 did not exhibit a glass-transition temperature ($T_g$). Since a weight loss of 5% ($T_{d5}$) for the BPy derivatives was observed at temperatures greater than 450 °C, the BPy derivatives' skeleton was probably not thermally decomposed below 450 °C.

The $^1$H NMR spectra of 4,4′-BPy3 and 6,6′-BPy3 are shown in **Figure 2**. The $^1$H NMR signals were assigned on the basis of $^1$H–$^1$H

COSY experiments (see **Figure S8** and **S9** in the **SI**). Interestingly, H-bonding was indicated by upfield shift of the CH protons (by 0.16 ppm for $H_a'$) and downfield shift of the CH protons (by 0.42 ppm for $H_b'$) when the compound was dissolved in chloroform-*d* ($CDCl_3$) solution. These results suggested that lone pairs of BPy core are probably shared by two protons in 6,6′-BPy3, whereas 4,4′-BPy3, the lone pair is occupied by only one proton, $H_a$. The CH···N H-bonding of 6,6′-BPy3 supports the planarity of the molecular framework in addition to the co-planarity of the BPy core. Similar trends were observed in the NMR spectra of the precursors of the BPy derivatives (see **SI**), confirming that this H-bonding interaction is a characteristic of the molecular core.

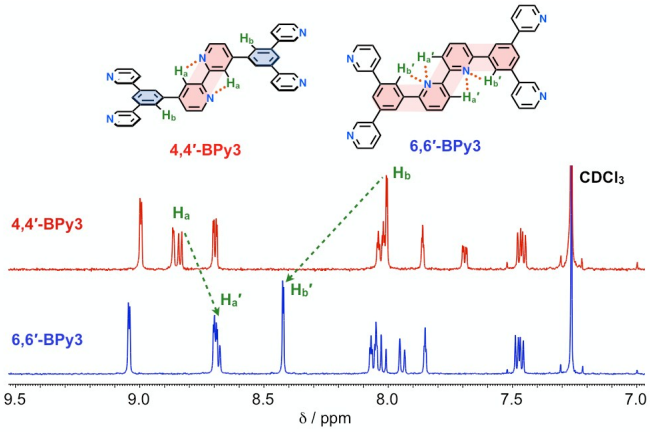


**Figure 2**. $^1$H NMR spectra of 4,4′-BPy3 and 6,6′-BPy3.

The molecular configurations of the BPy derivatives were also determined by X-ray crystallography (**Figure 3**). The X-ray structure of 4,4′-BPy3 exhibited a twisted core skeleton (BPy–phenyl dihedral angle = 37.0°). By contrast, the steric hindrance of the 6,6′-BPy3 core was reduced to 16.1°. The difference in these angles is attributed to the greater steric hindrance of the phenyl group attached at the 4,4′-positions of bipyridine compared to that of the phenyl group attached at the 6,6′-positions, in addition to the CH···N intramolecular H-bonding. These results are supported by both the DFT calculations and the NMR spectra (*vide supra*).

The unique packing structure of the crystal is also shown in **Figure 3**. Both compounds are stacked in an on-top array with π–π distances of 3.3–3.6 Å, which are as short as the sum (3.4 Å) of the van der Waals radius of carbon.

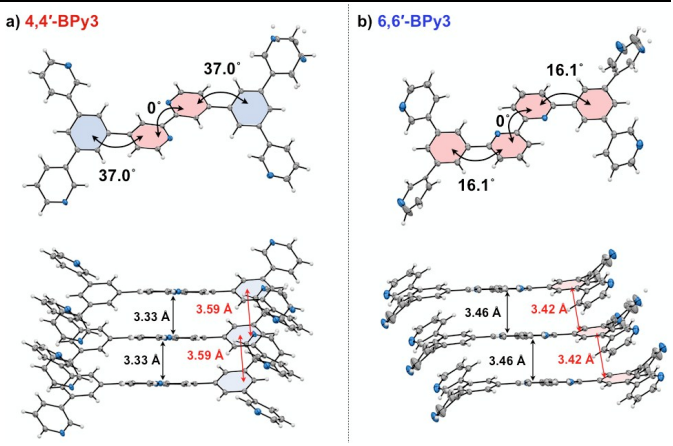


**Figure 3.** Crystal structures of a) 4,4′-BPy3 and b) 6,6′-BPy3: ORTEP diagrams and packing structures with thermal ellipsoids drawn at the 50% probability level.

In addition, intermolecular H-bonding interactions were confirmed at several outer peripheral pyridine rings (**Figure 4** and **Figure S13** in the **SI**). The obtained CH···N bond distances (2.61–3.14 Å) are reasonably classified as weak H-bonding and have already been reported in theoretical work on weak H-bonding distances between pyridine rings.[9] A large number of contributions of multi-furcated H-bonding can be an adequate trigger for the effective construction of the supramolecular structure. Furthermore, these H-bonding interactions strongly influence the physical properties of the BPy derivatives. To investigate the interaction of H-bonding, 4,4′-BPyPh and 6,6′-BPyPh were prepared as control molecules in which the compounds were substituted with benzene instead of the outer pyridine (see **SI**). These two types of molecules, with or without the ability to form hydrogen bonds, exhibited different retention factors ($R_f$s) in thin-layer chromatography (TLC) analysis on silica gel using chloroform/methanol (20:1 v/v) as an eluent and astonishingly different melting points ($T_m$s), despite the fact that their molecular weights are almost similar (see their synthesis and thermal properties in the **SI**).

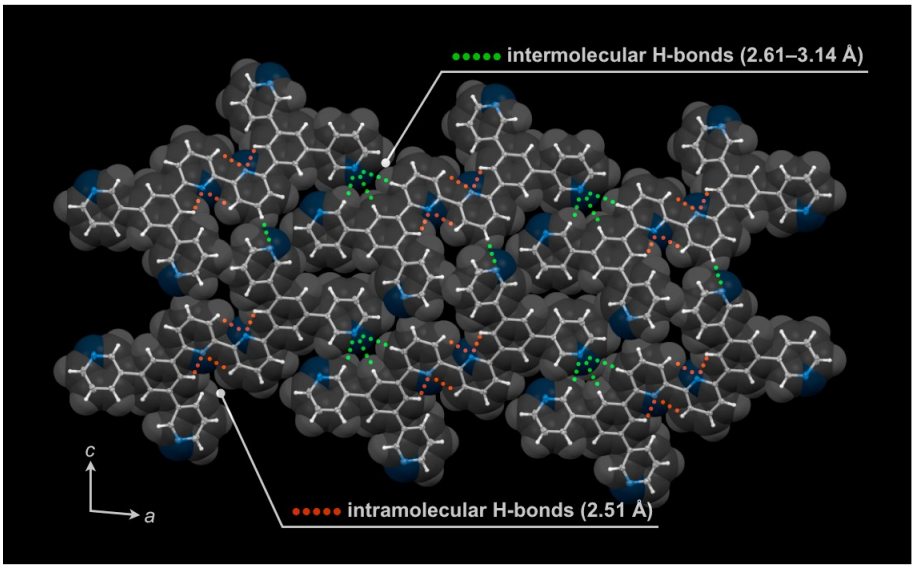


**Figure 4.** Crystal structures of 6,6′-BPy3: partially cutaway view focused on the intermolecular H-bonding network is illustrated with thermal ellipsoids drawn at the 50% probability level.

The UV–vis spectra of 4,4′-BPy3 and 6,6′-BPy3 in thin-film form were recorded (**Figure S15**). The spectra of the BPy derivatives showed a strong absorption band at 259 nm, derived from a π–π* transition. Interestingly, the absorption peak associated with the n–π* transition of bipyridine at approximately 320 nm is markedly enhanced in the 6,6′-BPy3 thin film, suggesting that the molecular structure of the 6,6′-BPy3 molecules is more planar than that of the 4,4′-BPy3 molecules in solid films. The optical band gap ($E_g$) of the BPy derivatives was estimated to be approximately 3.5 eV from the absorption edge. Notably, 6,6′-BPy3 exhibits a narrower band gap (3.5 eV) than 4,4′-BPy3 (3.6 eV) despite the only difference between them being their substituents. The ionization potential ($I_p$) of the BPy derivatives determined by photoelectron yield spectroscopy (PYS)[10] was approximately −6.5 eV (**Figure S16**), and the electron affinity ($E_a$) estimated from the $E_g$ and the $I_p$ was approximately −3.1 eV. The $E_a$ values of the BPy derivatives were deeper than that of TPBi (−2.8 eV), which is a conventional n-type semiconductor material for OLEDs.[11] These findings indicate that the BPy derivatives are suitable for both hole blocking and electron injection from the cathode metal. All the physical properties are summarized in **Table 1**.

**Table 1.** Electronic properties of BPy derivatives.

| Compound | $\lambda_{max}$ [a] (nm) | $I_p$ [b] (eV) | $E_g$ [c] eV) | $E_a$ [d] (eV) |
|---|---|---|---|---|
| 4,4′-BPy3 | 362 | –6.8 | 3.6 | –3.2 |
| 6,6′-BPy3 | 364 | –6.4 | 3.5 | –3.0 |

[a]$\lambda_{ex}$ = 260 nm. [b]$I_p$ was measured by photoelectron yield spectroscopy (PYS). [c]The $E_g$ was taken as the point of intersection of the normalized absorption spectra. [d]$E_a$ was calculated using $I_p$ and $E_g$.

To gain deeper insight into the amorphous thin-film structures, the molecular orientations of 100-nm-thick films were probed by VASE analysis. Because the very smooth surface of a bare Si substrate facilitates the molecular aggregation on the surface,[12] we inserted a typical host material, 4,4′-*N*,*N*'-dicarbazolylbiphenyl (CBP) between BPy films and bare Si substrate to avoid a crystallization of BPy derivatives caused by an excessive aggregation. We quantified the degree of orientation using the orientation parameter *S*, which is 0 when the transition dipole moments of molecules have a completely random orientation and is −0.5 when they have a completely horizontal orientation. The anisotropies of the refractive indices ($n$) and extinction coefficients ($k$) of the 100-nm-thick BPy films on Si/CBP (10 nm) are shown in **Figure 5**. In the VASE analysis of the organic bilayer films, we assumed that the optical constants ($n$ and $k$) of the inserted thin CBP film are the same as those of the 100-nm-thick CBP film on a bare Si substrate previously reported.[3a]

Consequently, the *S* values of 4,4′-BPy3 and 6,6′-BPy3 were estimated to be −0.28 and −0.32, respectively, which are substantially greater than that of the TPBi (−0.02).[5] This result demonstrates the high degrees of horizontal orientation of 4,4′-BPy3 and 6,6′-BPy3, which would create the advantage of carrier passes perpendicular to the substrate.

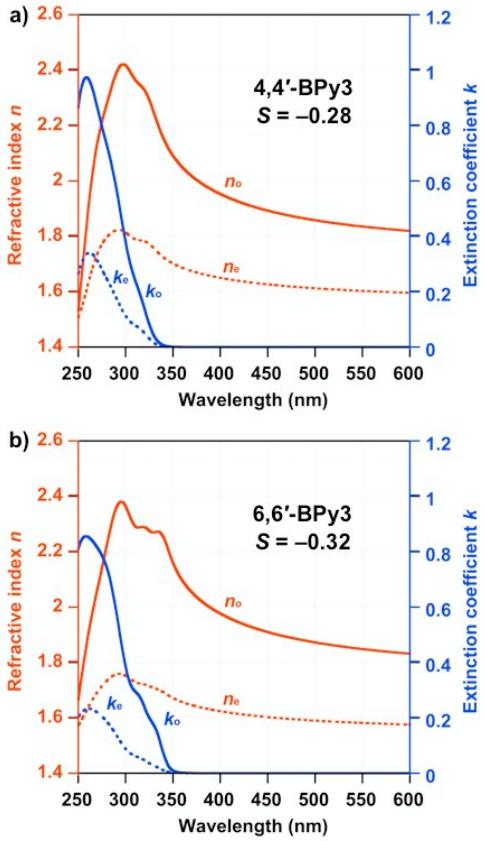


**Figure 5.** Anisotropies of the refractive indices (red) and extinction coefficients (blue) of a) 4,4′-BPy3 and b) 6,6′-BPy3 films. The solid and broken lines indicate the horizontal and vertical components of the optical constants, respectively.

To clarify the relationship between the carrier transport ability and molecular orientation, the former was determined by the time-of-flight measurement, whereas the carrier injection ability was qualitatively studied by temperature-dependent analysis of a carrier-only device.[13,14] We prepared films of 4,4′-BPy3 and 6,6′-BPy3 with thicknesses of 4.46 and 4.39 μm, respectively for use in TOF measurement. **Figure S17** shows the electron motilities of 4,4′-BPy3 and 6,6′-BPy3 films plotted as a function of the square root of the electric field. The electron mobility of 4,4′-BPy3 lies in the range from $1.5 \times 10^{-4}$ to $1.8 \times 10^{-4}$ $cm^{-2}$ $V^{-1}$ $s^{-1}$ at electric field strengths between $4.1 \times 10^{5}$ V $cm^{-1}$ and $8.2 \times 10^{5}$ V $cm^{-1}$. In comparison, as expected, 6,6′-BPy3 exhibited a higher electron mobility range: from $2.0 \times 10^{-4}$ to $3.0 \times 10^{-4}$ $cm^{-2}$ $V^{-1}$ $s^{-1}$ at electric field strengths between $4.0 \times 10^{5}$ V $cm^{-1}$ and $8.0 \times 10^{5}$ V $cm^{-1}$ (**Figure S17**). The electron mobility is almost one order of magnitude higher than that of TPBi.[13,15] Further, the energy barrier heights for the electron injection at the ETL and Al cathodes, as determined from the electron-only device characteristics at various temperatures, were 0.39 eV for TPBi, 0.34 eV for 6,6′-BPy3, and 0.26 eV for 4,4′-BPy3 (**Figure S18** and **S19**). These results qualitatively indicate that the insertion of BPy derivatives between the emissive layer and the Al electrode reduces the operating voltages of OLEDs.

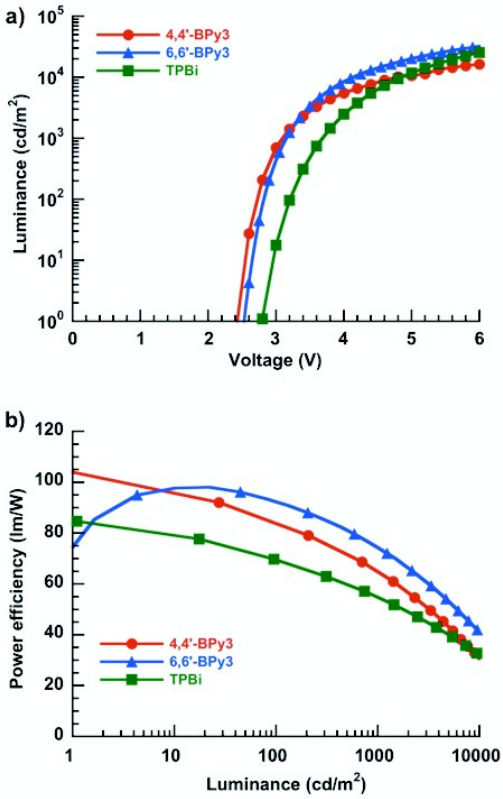


**Figure 6.** Performance of OLEDs with a device structure of [ITO (130 nm)/ triphenylamine-containing polymer: PPBI (20 nm)/TAPC (30 nm)/8 wt% $Ir(ppy)_3$-doped CBP (10 nm)/ETL (50 nm)/LiF (0.5 nm)/Al (100 nm)]: a) luminance–voltage characteristics and b) power efficiency–luminance characteristics.

Finally, we applied 4,4′-BPy3 and 6,6′-BPy3 as an ETM in OLEDs. To verify the performance of the Bpy derivatives, we fabricated $Ir(ppy)_3$-based OLEDs with a conventional device structure (**Figure S20**). The device structure was [ITO (130 nm)/ triphenylamine-containing polymer: 4-isopropyl-4′-methyldiphenyl-iodonium tetrakis(pentafluorophenyl)borate (PPBI)[16] (20 nm)/1,1-bis{4-[*N*,*N*-

di(*p*-tolyl)amino]-phenyl}cyclohexane (TAPC) (30 nm)/Ir(ppy)$_3$ 8 wt% doped CBP (10 nm)/ETL (50 nm)/LiF (0.5 nm)/Al (100 nm)]. As a reference, we used TPBi as an ETL. The operating voltage of these devices revealed a correlation of electron injection barrier height and electron mobility. In particular, the device with 6,6′-BPy3 exhibited low operating voltages of 2.5, 2.8, and 3.2 V at luminances of 1, 100, 1000 cd m$^{-2}$, respectively (**Figure 5a**). At 1000 cd m$^{-2}$, this device yielded a power efficiency ($\eta_{p,1000}$) of 74.3 lm W$^{-1}$, current efficiency ($\eta_{c,1000}$) of 74.6 cd A$^{-1}$, and external quantum efficiency ($\eta_{ext,1000}$) of 20.7% (**Figure 5b**, see also **Figure S21** in the **SI**). Compared with a TPBi-based device, the BPy derivatives-based devices exhibited operating voltages more than 0.5 V lower at 1000 cd m$^{-2}$, thus achieving a 1.2–1.3 times greater $\eta_{p,1000}$. All the device performances are summarized in **Table S6**.

In summary, we investigated the synergistic effect of molecular shape anisotropy and intermolecular H-bonding in the BPy derivatives on molecular orientation. Although the only difference between the BPy derivatives was the position of the substituents, we observed large differences in optical and electronical properties between them in their solution and crystal states. In addition, these structures led to highly horizontally oriented films induced by inter- and intramolecular H-bonding interactions. Furthermore, when installed as ETMs in OLEDs, the oriented films can deliver performance beyond that expected on the basis of their molecular formula.[17] We believe that this work provides a valuable strategy toward the development of smart OLED materials.

## Notes and references

‡Crystallographic data have been deposited with the Cambridge Crystallographic Data Center as supplementary publication no. CCDC 1433056 and 1433057. The data can be obtained free of charge from The Cambridge Crystallographic Data Centre *via* www.ccdc.cam.ac.uk/data_request/cif.

[1] a) J. Kido, M. Kimura, K. Nagai, *Science*. 1995, **267**, 1332–1334; b) Y. Sun, N. C. Giebink, H. Kanno, B. Ma, M. E. Thompson, S. R. Forrest, *Nature.* 2006, **440**, 908–912; c) D. Tanaka, H. Sasabe, Y.-J. Li, S.-J. Su, T. Takeda, J. Kido, *Jpn. J. Appl. Phys.* **2007**, *46*, 10–12; d) S. Reineke, F.Lindner, G. Schwartz, N. Seidler, K. Walzer, B. Lüssem, K. Leo, *Nature*. 2009, **459**, 234–238; e) M. G. Helander, Z. B. Wang, J. Qiu, M. T. Greiner, D. P. Puzzo, Z. W. Liu, Z. H. Lu, *Science,* 2011, **332**, 944–947; f) T.-H. Han, Y. Lee, M. R. Choi, S.-H. Woo, S.-H. Bae, B. H. Hong, J.-H. Ahn. T.-W. Lee. *Nat. Photonics,* 2012, **6**, 105–110; g) H. Uoyama, K. Goushi, K. Shizu, H. Nomura, C. Adachi, *Nature,* 2012, **492**, 234–238; h) H. Sasabe, H. Nakanishi, Y. Watanabe, S. Yano, M. Hirasawa, Y.-J. Pu, J. Kido, *Adv. Funct. Mater,* 2013, **23**, 5550–5555; i) H. Kaji, H. Suzuki, T. Fukushima, K. Shizu, K. Suzuki, S. Kubo, T. Komino, H. Oiwa, F. Suzuki, A Wakamiya, Y. Murata, C. Adachi, *Nat. Commun.* 2015, doi:10.1038/ncomms9476.

[2] a) D. Yokoyama, *J. Mater. Chem*. 2011, **21**, 19187–19202; b) K. -H. Kim, S. Lee, C.-K. Moon, S.-Y. Kim, Y.-Seo. Park, J.-H. Lee, J. W. Lee, J. Huh, Y. You, J.-J. Kim, *Nat. Commun.* 2014, **5**, 4769; c) M. J. Jurow, C. Mayr, T. D. Schmidt, T. Lampe, P. I. Djurovich, W. Brütting, M. E. Thompson, *Nat. Mater.* 2015, doi: 10.1038/NMAT4428.

[3] a) D. Yokoyama, A. Sakaguchi, M. Suzuki, C. Adachi, *Org. Electron.* 2009, **10**, 127–137; b) A. Wakamiya, H. Nishimura, T. Fukushima, F. Suzuki, A. Saeki, S. Seki, I. Osaka, T. Sasamori, M. Murata, Y. Murata, H. Kaji, *Angew. Chem. Int. Ed*. 2014, **53**, 5800–5804.

[4] a) S.-J. Su, H. Sasabe, Y.-J. Pu, K. Nakayama, J. Kido, *Adv. Mater.* **2010**, *22*, 3311–3316; b) H. Sasabe, D. Tanaka, D. Yokoyama, T. Chiba, Y.-J. Pu, K. Nakayama, M. Yokoyama, J. Kido, *Adv. Funct. Mater*. 2011, **21**, 336–342; c) D. Yokoyama, H. Sasabe, H. Furukawa, C. Adachi, J. Kido, *Adv. Funct. Mater*. 2011, **21**, 1375–1382; d) H. Sasabe, J. Kido, *Eur. J. Org. Chem*. 2013, 7653–7663; e) M. Liu, S.-J. Su, M.-C. Jung, Y. Qi, W.-M. Zhao, J. Kido, *Chem. Mater*. **2012**, *24*, 3817−3827.

[5] Y. Watanabe, H. Sasabe, D. Yokoyama, T. Beppu, H. Katagiri, Y.-J. Pu, J. Kido. *Adv. Opt. Mater.* 2015, **3**, 769–773.

[6] a) L. L. Merritt, E. Schroeder, *Acta Cryst.* 1956, **9**, 801. ; b) R.-J. Chein, E. J. Corey, *Org. Lett.* 2010, **12**, 132.

[7] a) M. Uchida, T. Izumizawa, T. Nakano, S. Yamaguchi, K. Tamao, K. Furukawa, *Chem. Mater.* 2001, **13**, 2680–2683; b) M. Ichikawa, N. Hiramatsu, N. Yokoyama, T. Miki, S. Narita, T. Koyama, Y. Taniguchi, *Phys. Stat. Sol. (RRL)*, 2007, **1**, No. 1, R37–R39; c) D. Yokoyama, A. Sakaguchi, M. Suzuki, C. Adachi, *Appl. Phys. Lett*. 2009, **95**, 243303; d) M. Ichikawa, T. Yamamoto, H.-G. Jeon, K. Kase, S. Hayashi, M. Nagaoka, N. Yokoyama, *J. Mater. Chem*. 2012, **22**, 6765.

[8] H. Sasabe, T. Chiba, S.-J. Su, Y.-J. Pu, K. Nakayama, J. Kido, *Chem. Commun*. 2008, 5821–5823.

[9] E. G. Hohenstein, C. D. Sherrill, *J. Phys. Chem. A* 2009, **113**, 878–886.

[10] H. Ishii, D. Tsunami, T. Suenaga, N. Sato, Y. Kimura, M. Niwano, *J. Surf. Sci. Soc. Jpn*. 2007, **28**, 264–270.

[11] J. Shi, C.W. Tang, C. H. Chen, *U.S. Patent 5646948*, 1997.

[12] D. Yokoyama, Y. Setoguchi, A. Sakaguchi, M. Suzuki, C. Adachi, *Adv. Funct. Mater.* 2010, **20**, 386–391.

[13] Y. Shirota, H. Kageyama, *Chem. Rev.* 2007, **107**, 953–1010.

[14] a) S. Dushman, *Phys. Rev*., **1923**, *21*, 623; b) O. W. Richardson, *Philos. Mag.*, **1924**, *28*. 633; c) M. Matsumura, T. Akai, M. Saito, T. Kimura, *J. Appl. Phys*, 1996, **79 (1)**, 264–268; d) W. Brütting, S. Berleb, A. Mückl, *Organic Electronics*, 2001, **2**, 1–36.

[15] a) T. C. Wong, J. Kovac, C. S. Lee, L. S. Hung, S. T. Lee, *Chemical Physics Letters.* 2001, **334**, 61–64; b) W. -Y. Hung, T. -H. Ke, Y. -T. Lin, C. -C. Wu, T. -H. Hung, T. -C. Chao, K. -T. Wong. C. -I. Wu, *Appl. Phys. Lett.* 2006, **88**, 064102.

[16] J. Kido, G. Harada, M. Komada, H. Shionoya, K. Nagai, *ACS Symp. Ser*. 1997, **672**, 381.

[17] Z. B. Henson, K. Müllen, G. C. Bazan, *Nat. Chem.* 2012, **4**, 699–704.

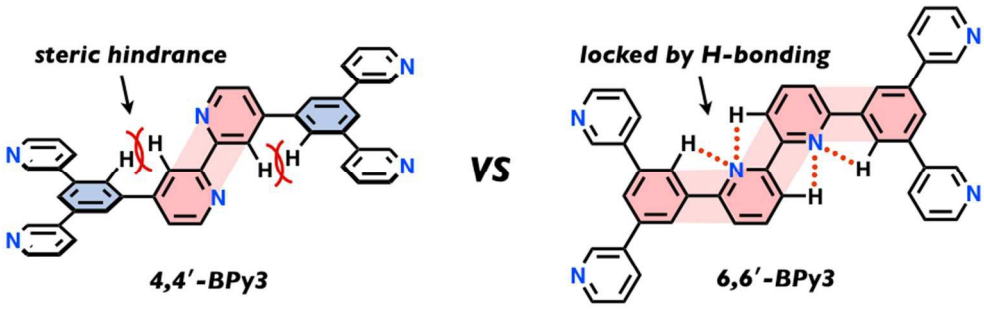


**Controlling the Anisotropy of Molecular Shape Induced by Bipyridine Skeleton**

338x159mm (72 x 72 DPI)